Hindawi
Advances in Polymer Technology
Volume 2022, Article ID 9741080, 20 pages
https://doi.org/10.1155/2022/9741080

*Research Article*

# Investigation of the Effect of Molecular Weight, Density, and Initiator Structure Size on the Repulsive Force between a PNIPAM Polymer Brush and Protein

**Getachew Tizazu**

*Department of Physics, Bahir Dar University, Kebele, 07 Bahir Dar, Ethiopia*

Correspondence should be addressed to Getachew Tizazu; getachewtizazu@gmail.com

Received 10 August 2022; Accepted 5 October 2022; Published 22 October 2022

Academic Editor: Pierre Verge



This paper focuses on the effect of degree of polymerization ($N$), density ($\sigma$), and pattern size ($x$) on the interaction force between a periodically patterned Poly(N-isopropylacrylamide) (PNIPAM) brush and protein. The hydrophobic interaction, the Van der Waals attractive force, and the steric repulsive force were expressed in terms of $N$, $\sigma$, and $x$. The osmotic constant (k1) and the entropic constant (k2) were determined from the fit of the steric repulsive force to an experimentally obtained force distance curve. The osmotic constant was 0.105, and the entropic constant was 0.255. Using these constants, the steric repulsive force was plotted as a function of the separation distance(s) between the substrate and the protein. The forces were determined at a separation distance equal to 0.3 nm, where L0 is the equilibrium thickness of the PNIPAM brush. At this separation distance, the value of the steric repulsive force was much higher than the value of the sum of the hydrophobic interaction and the Van der Waals attractive force for large degree of polymerization ($N > 100$) and density ($\sigma > 0.2$ chains/nm2). However, the repulsive force was comparable to the sum of the hydrophobic interaction and the Van der Waals attractive force for a small degree of polymerization ($N < 100$) and density ($\sigma = 0.2$). Furthermore, the steric repulsive force was plotted as a function of pattern size $x$. The plot indicated that the steric repulsive force becomes nearly zero for all degrees of polymerization and density when the value of the initiator structure size was less than 200 nm. In addition to the steric repulsive force, the lateral extension of the chains in the periodically patterned PNIPAM brush was calculated by scaling low and compared with the experimental data taken from previously published literatures. The polymer brush structure was modelled as if the immediate bare substrate is so wide that even a stretched polymer segment cannot reach to the next polymer brush structure. In such models, the value of the lateral extension was equal to the thickness of the homogenous brush. It was independent of the pattern size. However, when the polymer brush structure was modelled as if there is another polymer brush structure at a distance half of the size of the period, the lateral extension was found to be dependent on the size of the initiator structure size due to chain bridging. This was witnessed by the patterning of polymer brushes using the interferometric patterning of PNIPAM brushes and an atomic force microscopy imaging of the polymer brush structures both in air and in water. The polymer brush structure resolution in water was much lower than the resolution in air, which indicates the lateral extension of the polymer chains in water. For such kind of periodic polymer brush structures, the gap between them was calculated, and it was found dependent on the degree of polymerization, density, and initiator structure size.

## 1. Introduction

Poly(*N*-isopropylacrylamide) (PNIPAM) is a thermo-responsive polymer which undergoes a solubility switch at its lowest critical solution temperature (LCST) of 32°C, such that the polymer swells in water below the LCST, however, becomes less soluble and collapses above the LCST [1].

When the solvent temperature is changed to a value below the LCST, the PNIPAM segments repel each other and the long, flexible macromolecule adopts the fractal confirmation of a self-avoiding walk [2]. However, when the temperature is increased above the LCST, the effective repulsion between the segments of the polymer becomes zero, and the polymer adopts a Gaussian conformation [3].

Modification of solid surfaces by PNIPAM brushes has emerged as outstanding candidates for the fabrication of switchable surface; surfaces which can be changed from fouling to antifouling by an external stimulus [4]. The swelled PNIPAM brushes are antifouling while the collapsed ones are bioactive.

The mechanism of the antifouling nature of the PNIPAM brush below its critical temperature is due to the steric repulsion between the biomaterial and the polymer brush. When an adsorbate molecule such as a protein approaches a PNIPAM polymer brush in a good solvent below LCST, the surface polymer molecules become compressed. Compression results in decreased conformational entropy which is an unfavorable thermodynamic state. The system attempts to move back to the higher entropy state, repelling the adsorbate molecule. In addition, when a polymer chain is compressed by an adsorbate molecule, the local concentration of monomer units increases relative to the surrounding area, increasing the local osmotic pressure. Water molecules then diffuse to equalize the osmotic pressure, thereby repelling the adsorbate [5]. Repulsive forces between surface-anchored polymeric materials operate at intermediate separations, that is, 0.3–10 nm; the range of which is generally determined by the molecular weight and grafting density of the PNIPAM polymer [6]. On the contrary, if a protein approaches the PNIPAM polymer brush in a solvent above the LCST, the proteins attach to the surface since above the LCST the PNIPAM molecules are collapsed do not produce repelling forces. Therefore, PNIPAM surfaces can be switched from biorepelling to bioactive by changing the solution temperature. Figure 1 is a schematic showing PNIPAM polymer brush in solution switching from swollen to collapsed by changing the temperature, consequently reducing the steric repulsive force substantially.

There exist three main forces in the interaction of the PNIPAM brushes grafted onto solid surfaces and protein. The forces are steric repulsive force, Van der Waals attractive force, and hydrophobic attractive force. These forces can be obtained by differentiating the repulsive, Vander Waals, and hydrophobic energies, see Figure 2a. Figure 2b is a schematic of the model used to express the forces in terms of the thickness of the PNIPAM brush (L), and the distance between the protein and the PNIPAM brush surfaces (d). The model consists of a protein modelled as a sphere of radius R, a solvent (di water), grafted PNIPAM molecules, and a solid (substrate). A simple expression for the repulsive energy was formulated by Patel et al. for all solvent types. Equation (1) is the steric repulsive force which was obtained after differentiating the repulsive energy formulated by Patel et al. with respect to the nonequilibrium thickness of the polymer brush [9, 10].

$$F_R = \pi k_b T R^2 \frac{k_1}{a^2}\left((4\nu-1)\frac{k_2}{k_1}\right)^{1/4\nu}\frac{N\sigma^{2\nu+1/2\nu}}{(3\nu-1)}\left(\frac{(L)^{1/3\nu-1}}{(t)^{3\nu/3\nu-1}}-\frac{\nu(t)^{2\nu+1/3\nu-1}}{(3\nu-1)(L)^{4\nu-1/3\nu-1}}\right), \quad (1)$$

where $F_R$ is the repulsive force, $k_b$ is the Boltzmann constant, $T$ is the temperature, $R$ is the radius of the protein, $k_1$ is the undetermined coefficient for the osmotic term, $k_2$ is the undetermined term for the entropic term, $\nu$ is a term for the solvent condition, $N$ is the degree of polymerization, $\sigma$ is density, and $L$ is the equilibrium layer thickness of the grafted polymer brush.

The equilibrium thickness of the polymer brush is the thickness in the absence of the protein. It is the thickness where the osmotic and entropic force balance. Equation (2) is the equilibrium thickness obtained from the force minimization [9].

$$L = \left(\frac{k_1}{(4\nu-1)k_2}\right)^{3\nu-1/4\nu} \mathrm{aN}\sigma^{1-\nu/2\nu}. \quad (2)$$

The second type of force is the Vander Waals attractive force that operates at a very short distance. This force depends on the distance between the protein and the polymer brush, the polarizability of atoms, the refractive index, and the dielectric constants of the interacting materials, as well as the medium between them [12]. Equation (3) is the Vander Waals force between the PNIPAM polymer brush and the protein. It was obtained after differentiating the Vander Waals interaction free energy from Jeon et al. [10].

$$F_v = \frac{A}{6}\left(\frac{2R}{d(d+2R)}-\frac{R}{d^2}-\frac{R}{(d+2R)^2}\right), \quad (3)$$

where $A$ is the Hamaker constant, and $d$ is the distance between the polymer brush and the protein.

The third force that may contribute to the interaction of protein and the polymer brush is the hydrophobic interaction. Equation (4) is the hydrophobic interaction force between the polymer brush and the protein [10, 13, 14].

$$F_H = k_b T R e^{-d/14}. \quad (4)$$

In the fabrication of switchable surfaces, PNIPAM brushes are usually patterned to produce chemical and topographical gradients [15]. However, patterning causes a significant change in the morphology of the PNIPAM brushes [16]. Especially when the initiator structure size, $x$, is less than the degree of polymerization, $N$, the whole polymer brush structure is affected by stress relaxation due to the edge effects [17]. This is because the relaxation of the chains at the rim of the features creates extra room for neighboring chains further inside the polymer brush structure to relax by tilting away from the normal that decreases the maximum height of the polymer brush structure [18]. The decrease in the height of the polymer brush structure due to patterning affects the steric repulsive force since it depends on the thickness of the polymer brush structure. In addition, the relaxation of the chains at the rim of the polymer brush structure produces excess width when compared with that of the initiator structure size. Therefore, the total width of the polymer brush structure becomes the initiator structure size ($x$) plus the excess width ($w$) due to chain relaxation ($x + 2w$) [19]. Figure 3 is a schematic of the morphology of a PNIPAM polymer brush structure which shows the size

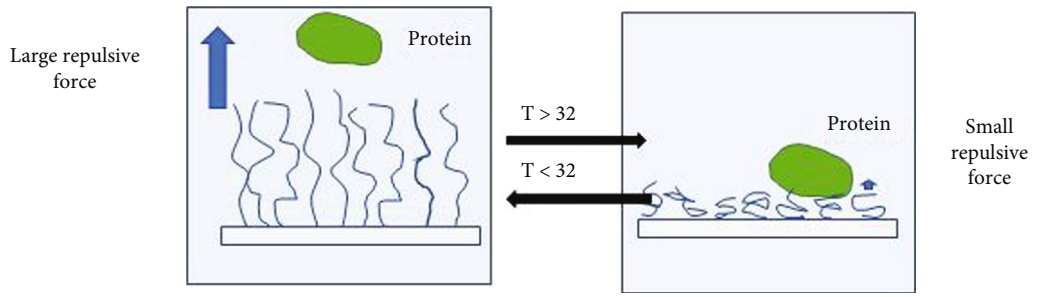


Figure 1: A schematic of PNIPAM polymer brush morphological changes due to change in solution temperature [7, 8].

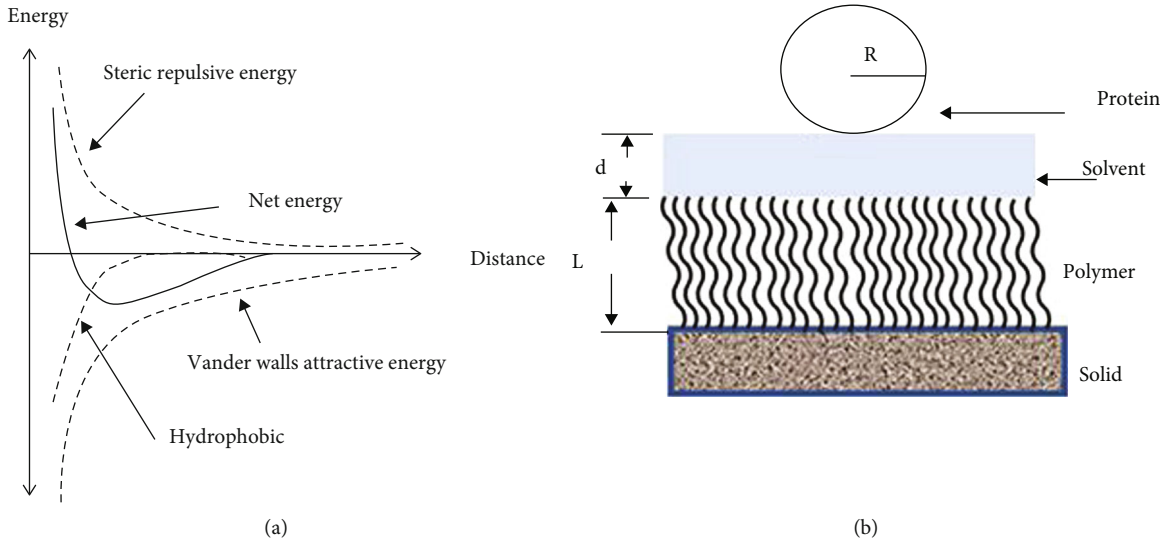


Figure 2: (a) A schematic of the interaction energies between the PNIPAM brush grafted onto a solid surface and the protein, and (b) is a schematic of the model used to determine the interaction forces [11].

of the excess width both above and below the LCST. Above the LCST, the polymer brush structures shirk and expose the bare substrate which makes it suitable for biomaterial deposition and below the LCST, it swells and covers the bare substrate [20].

Chain overlap occurs when the summation of the excess width (2 w) of two neighboring polymer brush structures is greater than the distance that separates the respective initiator structures, see Figure 3. Theoretically, the dimension of a single chain in the polymer brush structure is expressed as the combination of the tilting angle, $\theta$, which is measured from the normal, and the length of the chain, $l_i$. Consequently, the profile of the brush is defined by the set of points ($r_i$ and $h_i$) [15], where $r_i$ is the horizontal component, and $h_i$ is the vertical component of the PNIPAM chain. Equations (5) and (6) are the expressions for the two components as a function of angle from the normal and equilibrium thickness of a homogenous brush.

$$r_i = r_g + l_i \sin\theta, \tag{5}$$

$$h_i = l_i \cos\theta, \tag{6}$$

where $r_g$ is the distance between neighboring chains.

The angle is zero for the polymer chain at the middle, and it is 90 for the chain at the edge of the polymer brush structure. Therefore, the height of the central chain $h_0$ is equal to $l_0$, and the lateral extension is equal to $r_{90} = r_g + l_0$, where $l_0$ is the equilibrium polymer brush thickness given by Equation (2). In this paper, the relation between the degree of polymerization and the gap between periodic PNIPAM brushes in good solvent has been determined. This determination of key parameters will lead to the fabrication of efficient switchable surfaces because polymer brush structures can be programed by the polymerization time that controls the chain length, initiator density that is controlling the polymer brush density and controlling imitator structure size [22].

## 2. Methods

*2.1. Determination of the Repulsive Force between the Protein and the Polymer Brush.* For temperatures below the lowest critical temperature, the solvent parameter $v$ in Equation (1) was taken as 3/5 (good solvent) [23–25]. Equation (7) is the expression for the repulsive force in a good solvent or when the temperature of the solvent is below the LCST. When the solvent temperature is above the LCST, the solvent parameter, $v$, is equal to ½. Therefore, the expression

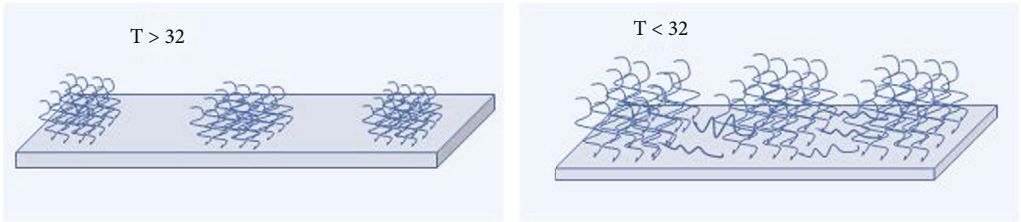


Figure 3: Schematic of the PNIPAM polymer brush structure in a solvent above the LCST and below the LCST [21].

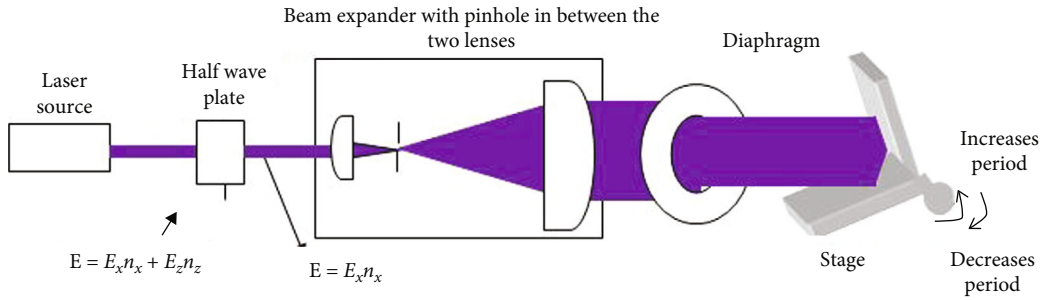


Figure 4: Setup for the interferometric lithography.

for repulsive force is changed to Equation (8).

$$F_r = k_b T \pi R^2 \frac{k_1}{a^2} \left(\frac{7k_2}{5k_1}\right)^{5/12} N \frac{5\sigma^{11/6}}{4L} \left[\left(\frac{L}{t}\right)^{9/4} - \left(\frac{t}{L}\right)^{3/4}\right], \tag{7}$$

$$F_r = k_b T \pi R^2 \frac{k_1}{a^2} \left(\frac{k_2}{k_1}\right)^{1/2} 2N \frac{\sigma^2}{L} \left[\left(\frac{t}{l}\right) - \left(\frac{l}{t}\right)^3\right]. \tag{8}$$

The equilibrium thickness has two expressions. Equation (9) is the expression for the polymer brush thickness when the temperature is below the LCST [26–28], and Equation (10) is the expression for the equilibrium thickness of the polymer brush when the temperature is above the LCST. The ratio of the equilibrium thickness below the LCST to the equilibrium thickness above the LCST is the swelling ratio ($\alpha$) given by Equation (11).

$$L_s = \left(\frac{5k_1}{7k_2}\right)^{1/3} \mathrm{aN}\sigma^{1/3} \text{ for } N > 1000 \text{ and } T < 32, \tag{9}$$

$$L_c = \left(\frac{k_1}{k_2}\right)^{1/4} \mathrm{aN}\sigma^{1/2} \text{ for } N > 1000 \text{ and } T > 32, \tag{10}$$

$$\alpha = \frac{L_s}{L_c} = \left(\frac{5}{7}\right)^{1/3} \left(\frac{k_1}{k_2}\right)^{1/12} \frac{1}{a\sigma^{1/2}}. \tag{11}$$

Besides, mostly, in an experimental investigation, the thickness of the polymer brush grafted on to the solid surface is reported. Thus, the degree of polymerization, $N$, and grafting density, $\sigma$, must be determined to calculate the interaction force. The degree of polymerization, N, and grafting density, $\sigma$, can be determined from the measured thickness using the relation given by Equations (12) and (13) [29].

$$N = \frac{h_w}{a} \left(\frac{h_w}{h_d}\right)^{1/2}, \tag{12}$$

$$\sigma = \left(\frac{h_d}{h_w}\right)^{3/2}, \tag{13}$$

where $h_d$ is the brush thickness above the LCST, $h_w$ is the brush thickness below the LCST, and $a$ is the monomer size which is equal to 0.5 nm.

In addition, the interchain distance, $d$, was calculated using Equation (14)

$$d = \sqrt{\frac{M_n}{N_A h \rho}} \text{ and } \sigma = \frac{a^2}{d^2}, \tag{14}$$

where $M_n$ is the number average molecular weight of the deposited film, $N_A$ is Avogadro's number, $h$ is the film thickness, and $\rho$ is the dry density of PNIPAM.

*2.2. Modelling the Attractive Forces between the Polymer Brush and the Protein.* In the Vander Waals force (Equation (3)), the components are protein, water, and polymer brush (Figure 2b). The homemaker constant, $A$, for this model is then [10].

$$A = \frac{3h\nu_e}{8\sqrt{2}} \frac{\left(n_1^2 - n_3^2\right)\left(n_2^2 - n_3^2\right)}{\left(n_1^2 + n_3^2\right)^{1/2}\left(n_2^2 + n_3^2\right)^{1/2}} \times \frac{1}{\left[\left(n_1^2 + n_3^2\right)^{1/2} + \left(n_2^2 + n_3^2\right)^{1/2}\right]} + \frac{3}{4} kT \frac{(\epsilon_1 - \epsilon_3)(\epsilon_2 - \epsilon_3)}{(\epsilon_1 + \epsilon_3)(\epsilon_2 + \epsilon_3)}, \tag{15}$$

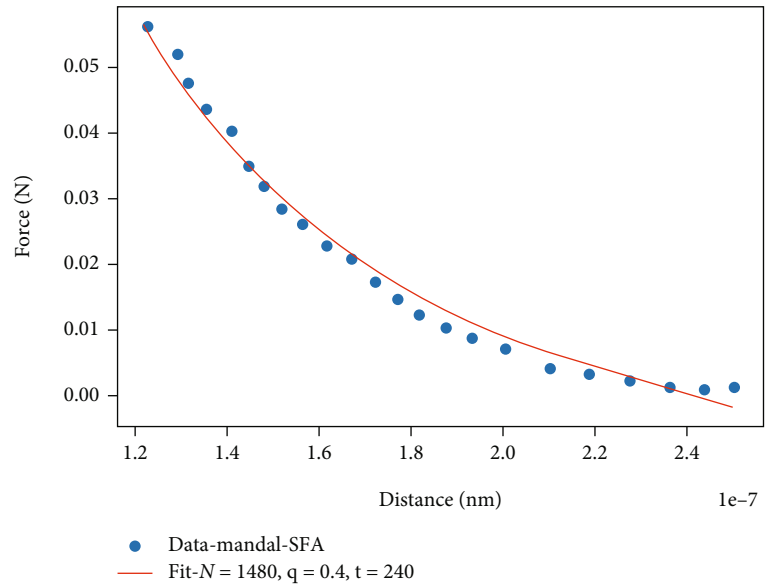


(a)

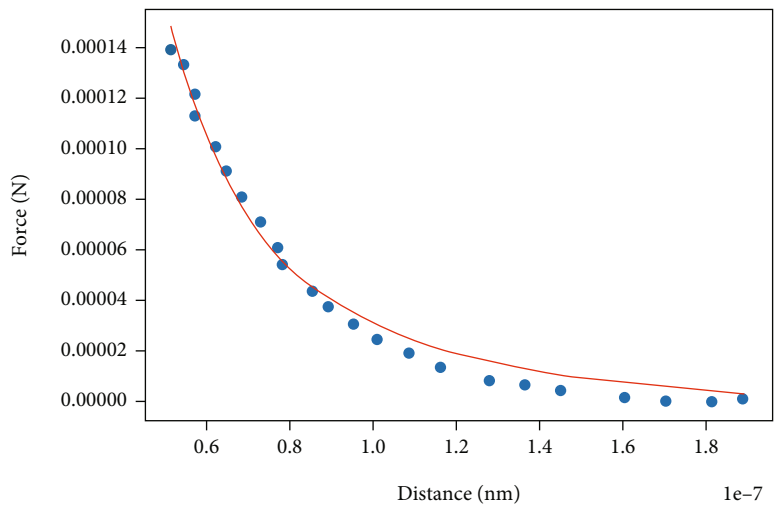


(b)

Figure 5: Continued.

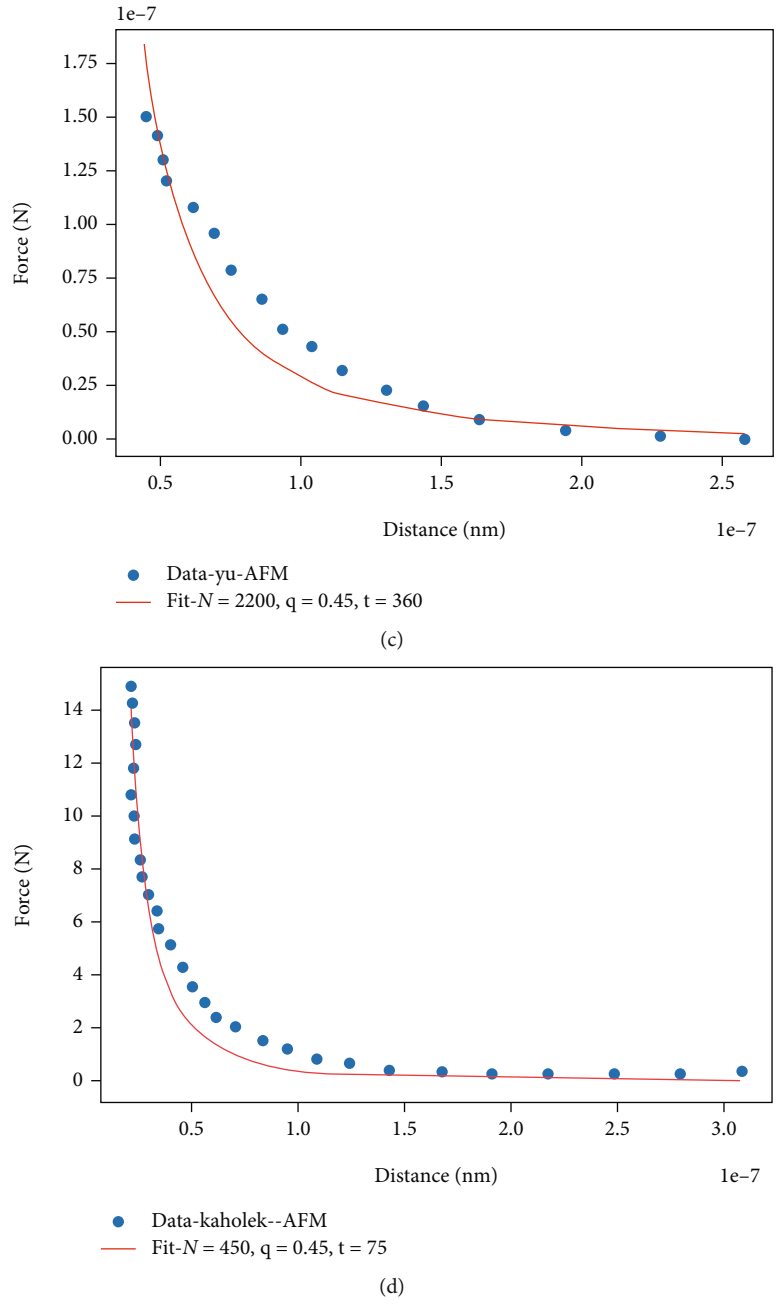


FIGURE 5: A plot of force versus distance for a PNIPAM polymer brush-coated mica and bare mica surface in water. Dots are experimental data digitized from ref [29, 34–37], and the solid line is a curve fitted to the data points (Equation (7)).

where $n1$, $n2$, and $n3$ are the refractive indices of protein, water, and PNIPAM polymer brushes, and $\varepsilon 1$, $\varepsilon 2$, and $\varepsilon 3$ are the static dielectric constants of protein, water, and PNIPAM polymer brushes, respectively. The values of the refractive index and the dielectric constants were taken from [30]. [10], and they are equal to $n_1 = 1.539$, $n_2 = 1.33$, $n_3 = 1.5$, $\epsilon_1 = 2.64$, $\epsilon_2 = 79.69$, and $\epsilon_3 = 2.26$. The homemaker constant was determined after substituting these values in Equation (16), and it was equal to -5.8, and therefore, the Vander Waals force between the polymer brush and the protein is written as

$$F_v = \frac{-5.8}{6}\left(\frac{2R}{d(d+2R)} - \frac{R}{d^2} - \frac{R}{(d+2R)^2}\right). \quad (16)$$

The total attractive force ($F_{\mathrm{Ta}}$) is then the sum of the

Table 1: Calculated k1 and k2 values.

| K1 | K2 | Density chain/ nm$^2$ | Polymerization ($N$) | Measured thickness in air | Measured thickness in water | Calculated thickness | Ref | $R^2$ |
|---|---|---|---|---|---|---|---|---|
| 0.018 | 0.037 | 0.4 | 1480[C] | 74 nm[a] | 240 nm[b] | 261 nm | [d]Mandal | 0.88 |
| 0.065 | 0.115 | 0.45 | 2200 | 170 nm | 360 nm | 352 nm | [e]Yu | 0.90 |
| 0.105 | 0.255 | 0.43 | 2330 | 125 nm | 270 nm | 290 nm | [d]Plunket | 0.99 |
| 0.086 | 0.126 | 0.14 | 4080 | 70 nm | 210 nm | 171 nm | [d]Malhan | 0.97 |
| 0.05 | 0.225 | 0.45 | 450 | 25 nm | 75 nm | 73 nm | [f]Kaholek | 0.95 |

[d] the force-distance curve was obtained using a surface force apparatus which consisted of PNIPAM brushes grafted on freshly-cleaved mica and a bare mica sheet. [e] The force versus separation curve was measured with the AFM colloid (6 um in diameter) probe upon approaching the PNIPAM brush grafted onto a silicon substrate. [f] The force versus distance curve was measured using AFM tip modified with PNIPAAM brushes while approaching a PNIPAM brush modified substrate (the polymerization time was 5- and 60-min for the substrate and cantilever, respectively).

Vander Waals force and the hydrophobic force.

$$F_{\mathrm{Ta}} = \frac{-5.8}{6}\left(\frac{2R}{d(d+2R)} - \frac{R}{d^2} - \frac{R}{(d+2R)^2}\right) - k_b T R e^{d/14}. \tag{17}$$

The total interaction force is the sum of the repulsive and attractive forces

$$F_T = k_b T \pi R^2 \frac{k_1}{a^2}\left(\frac{k_2}{k_1}\right)^{1/2} 2N\frac{\sigma^2}{L_c}\left[\left(\frac{t}{l_c}\right) - \left(\frac{l_c}{t}\right)^3\right] - \frac{5.8}{6}\left(\frac{2R}{d(d+2R)} - \frac{R}{d^2} - \frac{R}{(d+2R)^2}\right) - k_b T R e^{-d/14}. \tag{18}$$

*2.3. Effect of Patterning on the Interaction Force.* For a polymer brush structure, the expression for the equilibrium thicknesses is proposed to have a relation with the initiator structure size ($x$), initiator density ($q$), and the brush height at large initiator structure size ($h_h$) [31].

$$L_p = h_h q^{1/3} f_1(x), \tag{19}$$

where $f_1(x)$ is a function that depends on the initiator structure size, which will be determined from the curve fitting of an experimental data.

Therefore, due to the reduction of density and equilibrium thickness for polymer brush structures, the equation for the steric repulsive force is modified to include the effect of patterning, Equation (20).

$$F_p = k_b T \pi R^2 \frac{k_1}{a^2}\left(\frac{7k_2}{5k_1}\right)^{5/12} N\frac{5}{8L_p}\left(\frac{\sigma}{2}\right)^{11/6}\left[\left(\frac{2L_p}{t}\right)^{9/4} - \left(\frac{t}{2L_p}\right)^{3/4}\right]. \tag{20}$$

*2.4. Chain Overlap between Neighboring Polymer Brush Structures.* For the dense polymer brush, $r_g$ in Equation (5) is too small compared to the excess width, thus, for a dense brush $r_{90}$ is equal to $l_0$ which is the equilibrium thickness of the PNIPAM brush. The horizontal component of the chain end-to-end distance below the LCST is then equal to

$$r_i = r_g + \left(\frac{5k_1}{7k_2}\right)^{1/3} \mathrm{aN}\sigma^{2/5} \sin\theta. \tag{21}$$

*2.5. Patterning of PNIPAM Brushes.* Polymer brushes were prepared by atom transfer radical polymerization. Brush thickness was controlled by the polymerization time. Periodic patterns of PNIPAM brush structures grafted on silicon oxide substrates were fabricated using interferometric lithography; the Lloyds' mirror setup was used in the interferometric lithography since it is easy to setup and uses the same light source (beams are coherent), Figure 4 [32, 33]. The 266 nm laser from coherent was used as the light source. The period of the polymer brush structure fabricated by the interference of two coherent plane waves is given by Equation (22), and the normalized intensity distribution of the beams is given by Equation (23). The period can be increased or reduced by changing the angle between the two beams.

$$d = \frac{\lambda}{n\,2\sin(\theta/2)}, \tag{22}$$

$$I(s) = 1 + \cos\left(\frac{2\pi}{d}s\right), \tag{23}$$

where $d$ is period, $\lambda$ is the exposing wave length, $n$ is refractive index of the medium, $\theta$ is the angle between the beams, and $s$ is the distance from the joint.

The polymer brush structures were characterized by atomic force microscopy using a Nanoscope III, Digital Instruments, Santa Barbra, CA. A home built heating stage was used to heat the samples while imaging in water. The heating stage consists of a Peltier crystal from Marlow Industries Inc., an insulator mounted on an AFM sample disc and a DC power supply. The temperature was controlled by an omega132 temperature controller.

*2.6. Data Extraction from Published Journals.* To calculate the steric repulsive force between the proteins and the PNIPAM polymer brush, the osmotic ($k_1$) and entropic ($k_2$) proportionality constants were determined by digitizing data

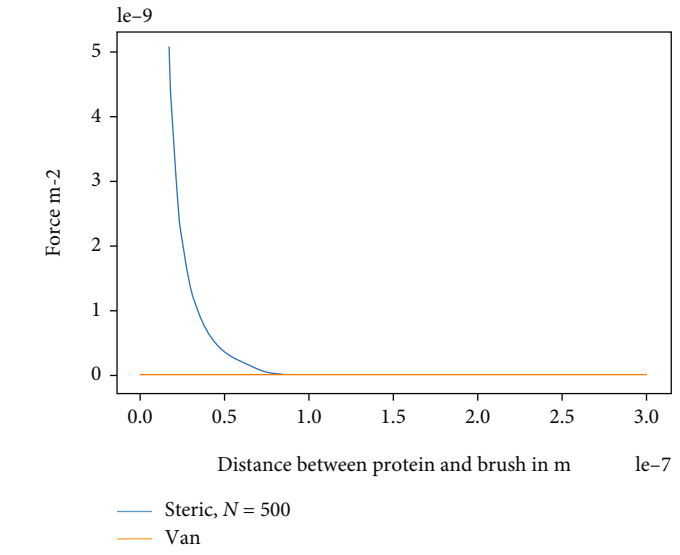


(a)

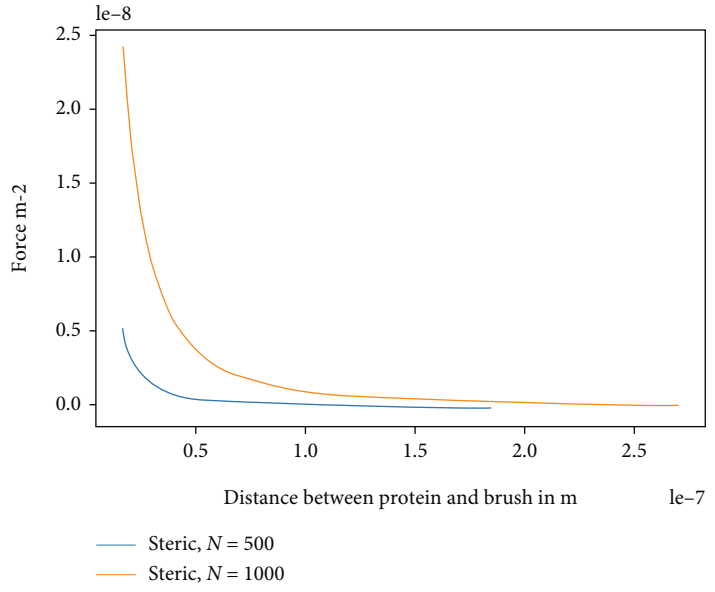


(b)

Figure 6: Continued.

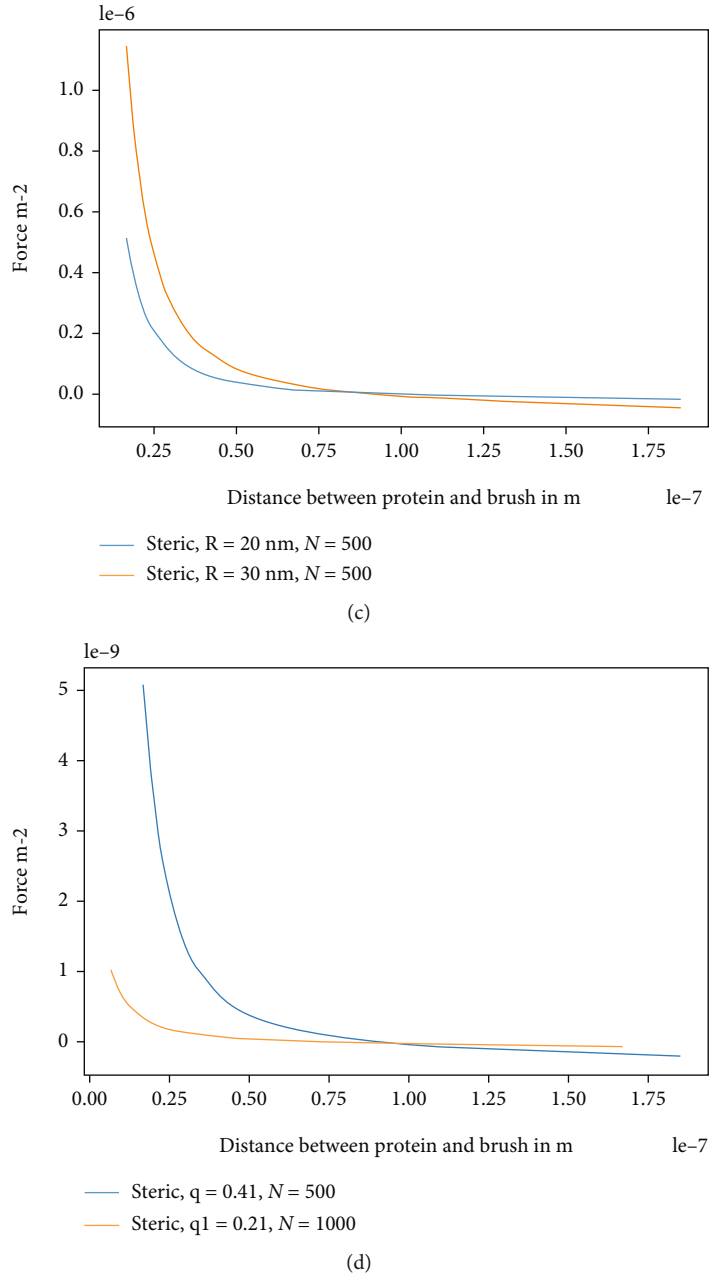


FIGURE 6: Plot of force as a function of the distance between the polymer brush and protein. (a) plot of the Vander Waals and repulsive forces. (b) Plot of the steric repulsive force for different degrees of polymerization. (c) Plot of the steric repulsive force for different sizes of proteins. (d) Plots of the steric repulsive force for different densities.

from previously reported force distance curves [29, 34–37]. This was done since the $k_l$ and $k_2$ values of PNIPAM in water are not available in the literature. In addition, the unknown functions, $f_1$ in the equilibrium thickness and $f_2$ in the excess width of the polymer brush structures, were determined from digitized and replotted data [31, 38] .To collect these data of Poly(N-isopropylacrylamide) brushes, google scholar (2000 to 2021) was searched using the following keywords: thermoresponsive patterned substrate, force-distance curves of Poly(N-isopropylacrylamide) brushes, scaling law, swelling ratio, and Poly(N-isopropylacrylamide) brushes.

## 3. Results and Discussion

*3.1. Determination of the Osmotic and Entropic Constants of the Repulsive Force.* To obtain the osmotic and entropic constants, Equation (7) was fitted to a digitized data from references [29, 34–37]. Figure 5(a)–5(d) is a python plot of force-distance curves which are fitted to the repulsive force (Equation (7)) using SciPy optimize. In the process of fitting, the value of the nonequilibrium thickness was varied from 0.4 L to 0.95 L because the nonequilibrium thickness is always less than the equilibrium thickness [25, 39]. The

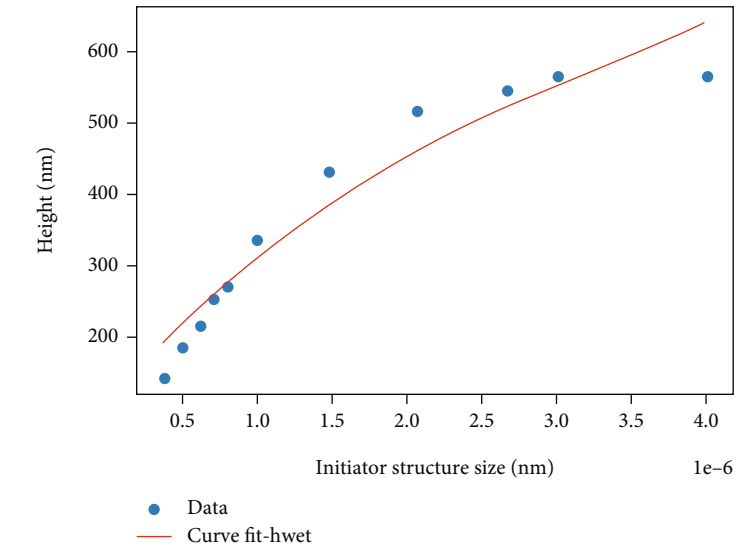


(a)

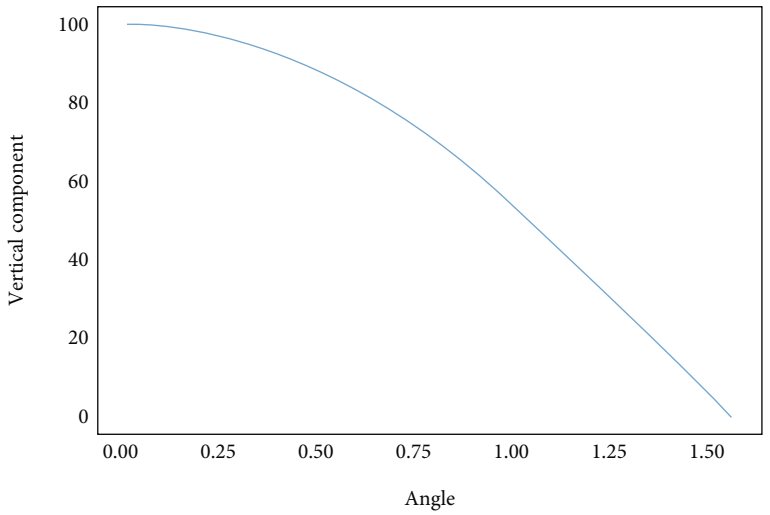


(b)

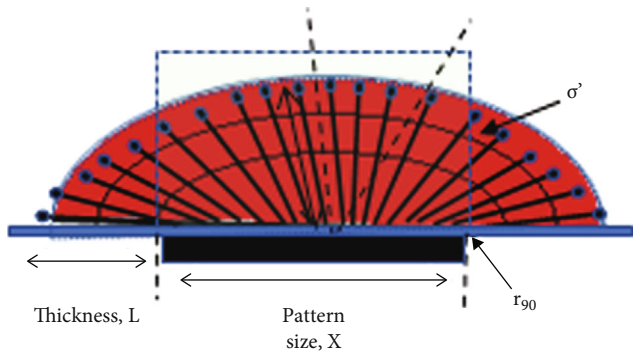


(c)

Figure 7: Continued.

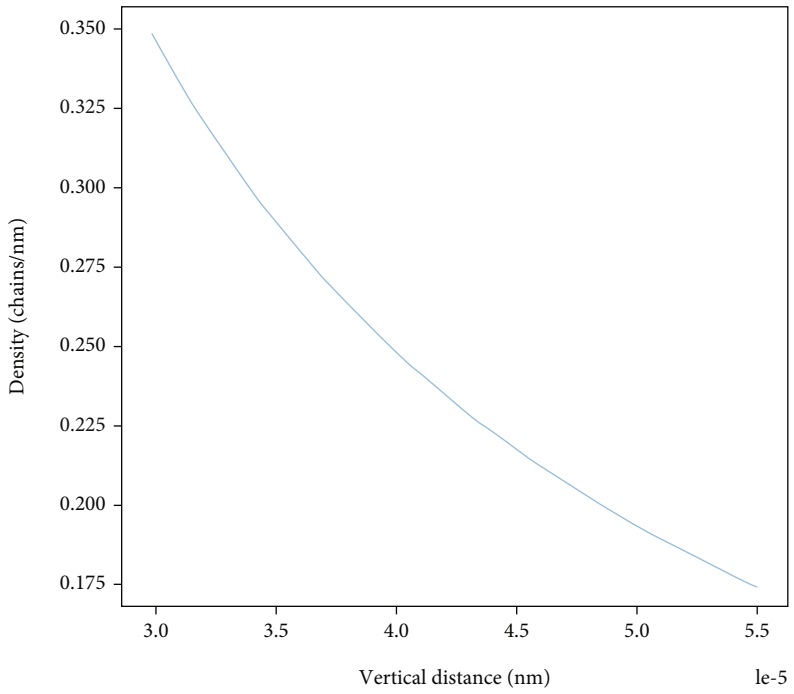


(d)

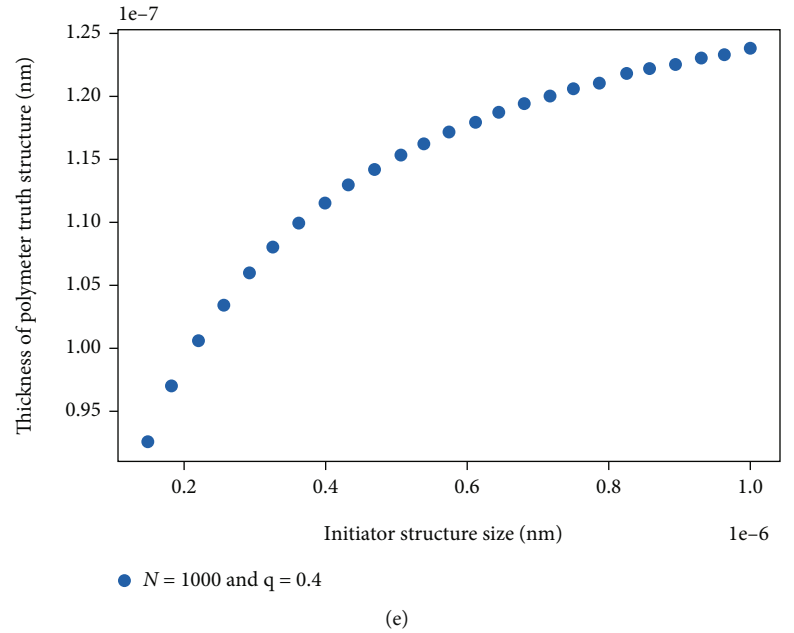


(e)

Figure 7: Continued.

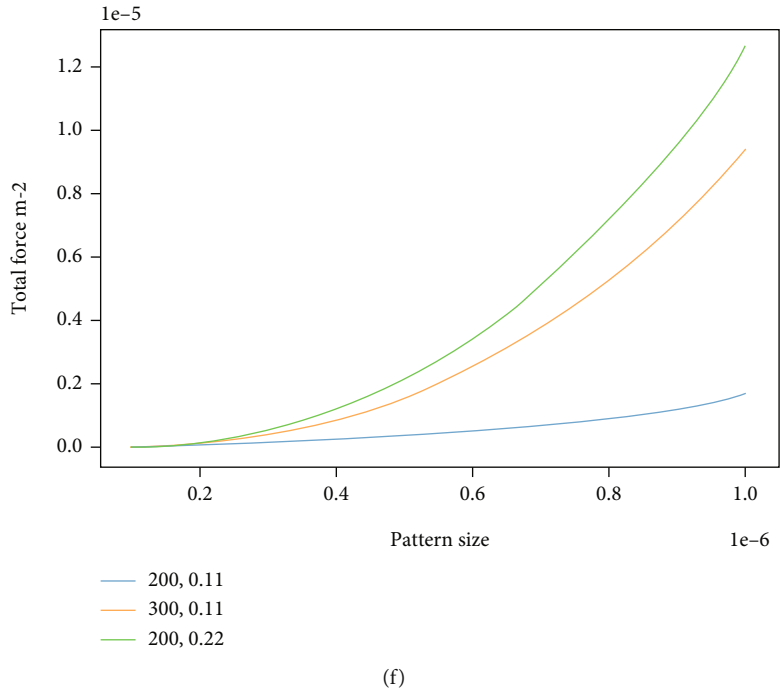


(f)

Figure 7: (a) plot of height of the PNIPAM polymer brush structure grafted on silicon oxide substrate versus initiator structure size and (b) plot of the vertical component (Equation (6)) of a polymer chain in the structure as a function of the tilting angle. (c) is a schematic of the constant density lines for the polymer brush structures grown from an initiator structure size, $x$, and the orientation of the polymer chains in the polymer brush structure (d) is plot of density of the polymer brush structure as a function of height, (e) is plot of the height of the polymer brush structure as a function of initiator structure size, and (f) is a plot of the repulsive force versus initiator structure size for different degrees of polymerization and density.

maximum compression (0.4 L) was estimated from the density and the equilibrium thickness which is equal to $\sigma L$. And the maximum value of the nonequilibrium thickness of the polymer brush is estimated as 0.95 L or can be estimated by L-0.3 nm, where 0.3 nm is the monomer size. In the process of fitting, the difference between the model's predictions and the data was calculated and minimized over several iterations while varying the parameters $k_1$ and $k_2$. Each time the code is running, the parameters are modified to determine new values that provide a better agreement between the model prediction and the experimental data. It should be pointed out that the difference in force curves between the theoretical and experimental is that the theoretical curve provides purely the interaction forces between a protein and the surface, whereas the experimental force measurements contain both protein-surface interactions and hydrodynamic forces. The calculated results for each data are presented in Table 1. The values chosen from the table are $k_1 = 0.105$ and $k_2 = 0.255$ with an R-square value of 0.99. These values were chosen for further investigation of the steric repulsive force for both homogenous and patterned PNIPAM brushes. To validate the values of $k_1$ and $k_2$, the equilibrium layer thickness was determined using Equation (9) and compared with the experimentally measured thickness. The experimentally reported layer thickness, $L_0$ is about 270 nm, and the theoretically calculated equilibrium layer thickness (Equation (9)) using the values of $k_1$ and $k_2$ is about 290 nm, which are in relatively good agreement with the experimental results. The difference in the calculated thickness and the experimental value is due to the relation that was derived for the moderate density regime [40, 41].

*3.2. Comparison of the Attractive and Repulsive Forces.* PNIPAM polymer brush surfaces are hydrophobic below the LCST and hydrophilic above the LCST [42]. The hydrophobic attraction force contributes to the interaction force when the surface is hydrophobic, that is, when the solvent temperature is above 32. Therefore, in the comparison of the attractive and repulsive force between the polymer brush and the protein, only the Vander Waals and steric repulsive forces were considered. In addition, the distance between the PNIPAM surface and the protein under the condition of no adsorption was taken as 0.3 nm, which is almost the same as the PNIPAM monomer size [43]. To examine the effect of Vander Waals on steric repulsion below the LCST, the two forces were plotted as a function of the distance between the protein and PNIPAM surface. Figure 6(a) is a plot of the Vander Waals and steric repulsive forces as a function of the distance between the polymer brush and protein. The Vander Waals force is nearly zero when compared with the steric repulsion force. This is in agreement with Sheth and Leckband who reported that for a surface grafted homogenous polymer brush, whose height is greater than 10 nm, the contribution of the Vander Waals is almost zero [43]. Therefore, for PNIPAM polymer brush in a solvent below the LCST, the total force between the polymer brush and the protein

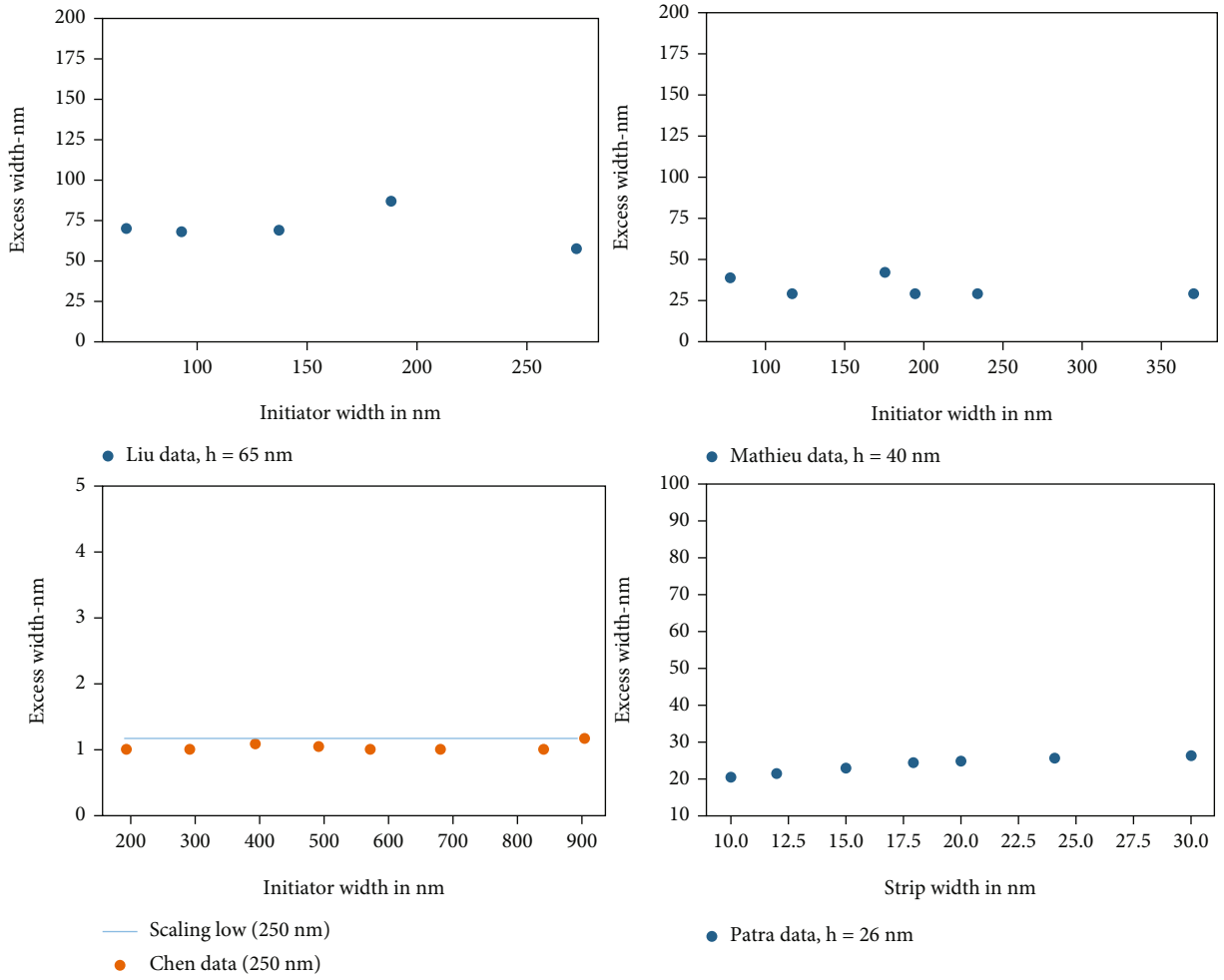


Figure 8: Plots of excess width of the polymer brush structure versus initiator structure size (primary data were taken from references [15, 16, 19, 21], and the plotted data (the excess width) was calculated using Equation (26).

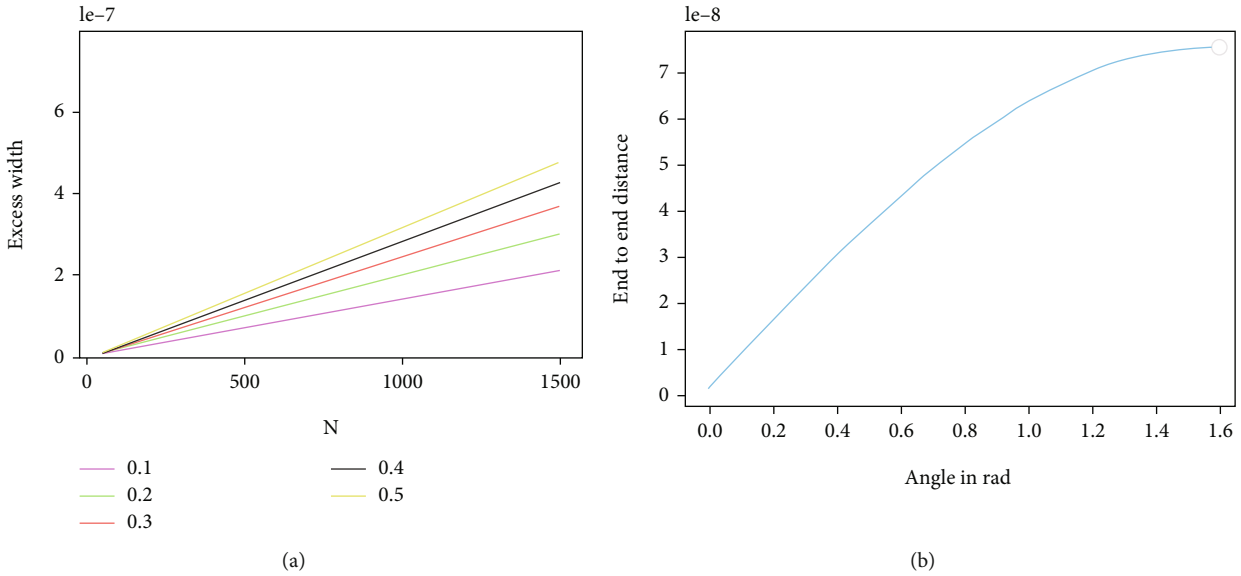


Figure 9: (a) is a plot of the excess width of a polymer brush structure versus the degree of polymerization for different densities; (b) plot of the horizontal component of a polymer chain in the polymer structure, Equation (23).

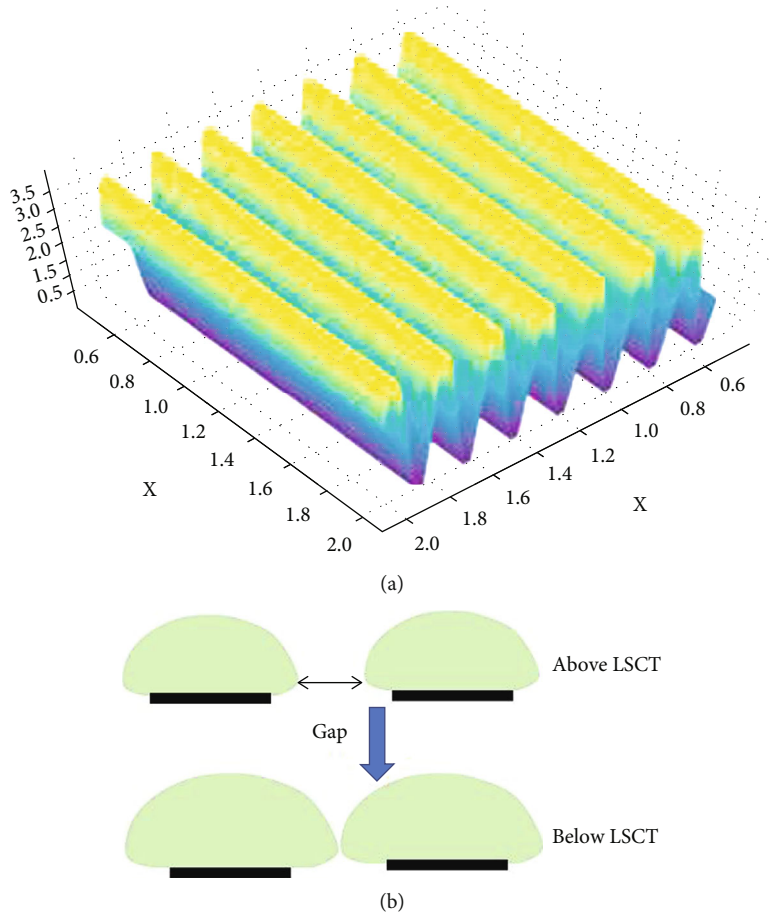


Figure 10: (a) a contour plot of the patterning intensities during interferometric patterning; (b) the schematic of the excess width grown on the patterned surface.

is dominantly the repulsive force. This repulsive force is dependent on the degree of polymerization density and protein size as can be seen in Figure 6(b)–6(d). When the degree of polymerization increases from 500 to 1000, the repulsive force also increases (Figure 6(b)). In addition, when the protein size increases from 20 nm to 30 nm, the repulsive force also increases (Figure 6(c)). The effect of the grafting density of the polymer brush on the steric repulsive force is insignificant when compared with the degree of polymerization (Figure 6(d)).

*3.3. The Repulsive Force for Patterned PNIPAM Brush Surfaces.* The repulsive force depends on the height of the polymer brush structure. Therefore, to determine the repulsive force for patterned polymer brush surfaces, first the relation between the height of the polymer brush structure and the initiator structure size must be determined. Figure 7(a) is a plot of the height of a PNIPAM polymer brush structure ($l_p$) versus initiator structure size ($x$). The data was digitized from references [31, 38] and replotted using Matplotlib. The plot was then fitted with Equation (19) to obtain $f_1(x)$, and the fit equation was equal to

$$l_p = h_w q^{1/3}\, bx^n, \tag{24}$$

where $b$ and $n$ are the fitting parameters, and they are equal to $4.6 \times 10^5$ and 0.5, respectively. The homogenous brush height ($h_w$) and the initiator density ($q$) were obtained from the data source, and they are equal to 562 nm and 1, respectively.

As can be seen in the figure (Figure 7(a)), the height of the polymer brush structure decreases as the initiator structure size decreases due to the relaxation of the chains at the rim, which creates extra room for neighboring chains further inside the polymer brush structure to tilt away from the normal increasing its entropy [18]. This tilting away of the chains from the normal causes a decrease in the density which consequently decreases height of the polymer brush structure. The profile of a single polymer chain in the nanostructured brush was defined by the set of points ($r_i$ and $h_i$), where $r_i$ is the horizontal component, and $h_i$ is the vertical component. The vertical component was plotted to investigate the effect of chain tilting on the height of the brush. Figure 7(b) is the plot of the vertical component (Equation (6)) of a polymer chain in the structure as a function of the tilting angle. The vertical component is given in terms of % of equilibrium thickness, and the angle is given in radians. As the tilting angle increases, that is, as the grafting site moves away from the center of the polymer brush

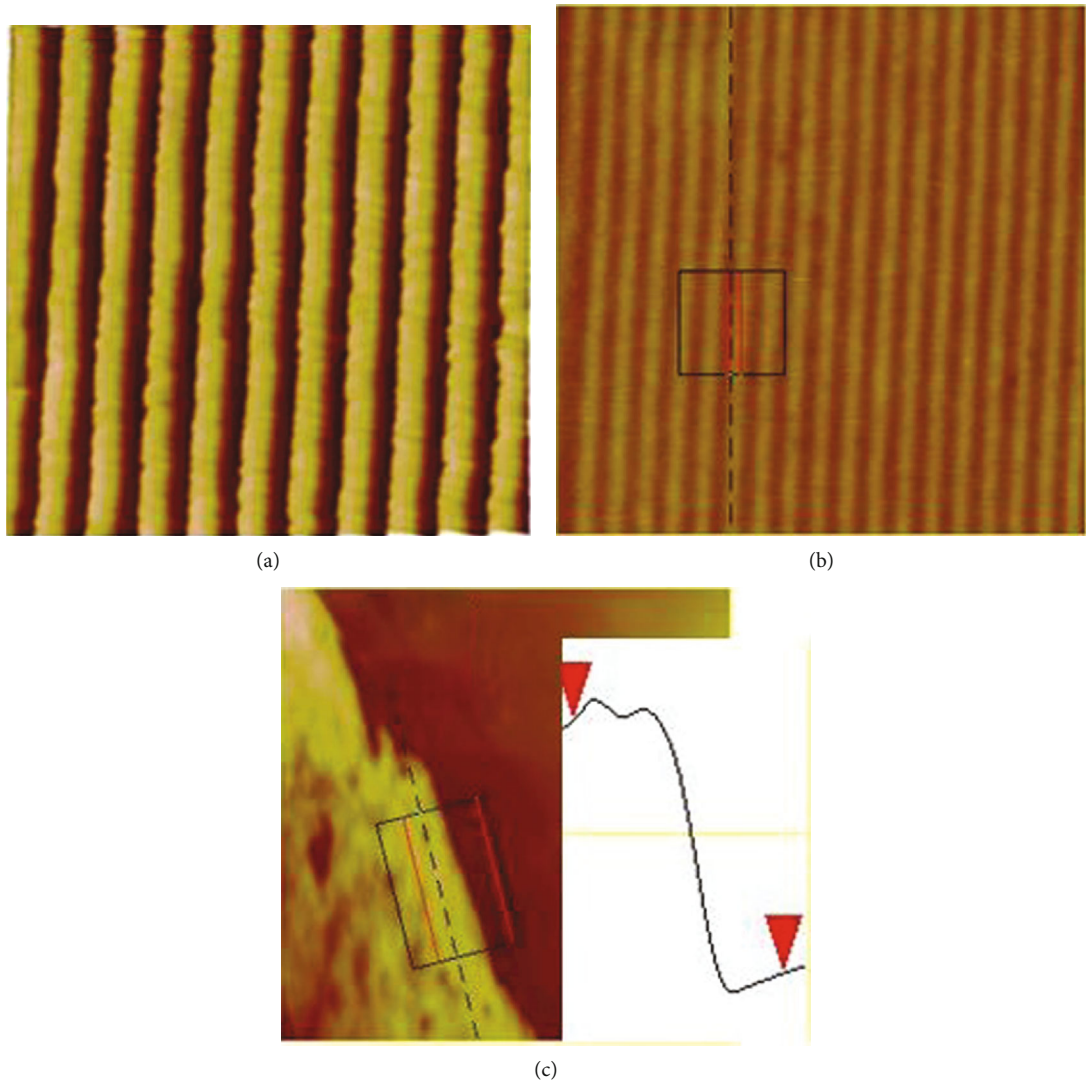

(a) (b) (c)

Figure 11: (a) Atomic force microscopy image of PNIPAM brush structure 25°C; (b) at 36°C; and (d) atomic microscopy image of a scratched polymer brush with its thickness.

structure, the vertical component decreases and finally becomes zero. Therefore, in a good solvent, the polymer brush structure will have a lens like morphology which its surface can be approximated by an ellipse of minor axis $L_0$ and major axis $x/2 + L_0$, where $L_0$ is the equilibrium thickness of the brush in a good solvent, and $x$ is the initiator structure size. The density of the polymer brush structure, $\sigma^{'}$, in terms of the density of the homogenous brush, $\sigma_0$ (where all the brush are assumed vertically upward direction) can be obtained using the Ramanujan formula of the perimeter of the ellipse which is

$$p = \pi\left\{3\left(2L + \frac{x}{2}\right) - \sqrt{\left[\left(4L + \frac{x}{2}\right)\left(4l + \frac{3x}{2}\right)\right]}\right. . \quad (25)$$

Since the number of chains, $n$, grafted on to the initiator size $x$ is conserved, then number of chins $(n) = \sigma 0x = \sigma^{'} p$. Solving for $\sigma^{'}$ and taking the average density at half of the polymer brush structure height (replacing L by L/2) yields Equation (26)

$$\sigma' = \frac{\sigma_0 x}{1/2\pi\{3(2L + (x/2)) - \sqrt{[(4L + (x/2))(4l + (3x/2))]}} . \quad (26)$$

After substituting the modified density in to Equation (9), the height of the polymer brush structure is then equal to

$$L_p = \left(\frac{5k_1}{7k_2}\right)^{1/3} \mathrm{aN}\sigma'^{1/3} . \quad (27)$$

Figure 7(c) is a schematic of the constant density lines for the polymer brush structures and the orientation of the polymer chains in the polymer brush structure. The shaded rectangle with sides equal to $x$ and $L_0$ is the polymer brush structure when the chains do not relax, and the elliptical shape is the equilibrium shape after the brush relaxes on

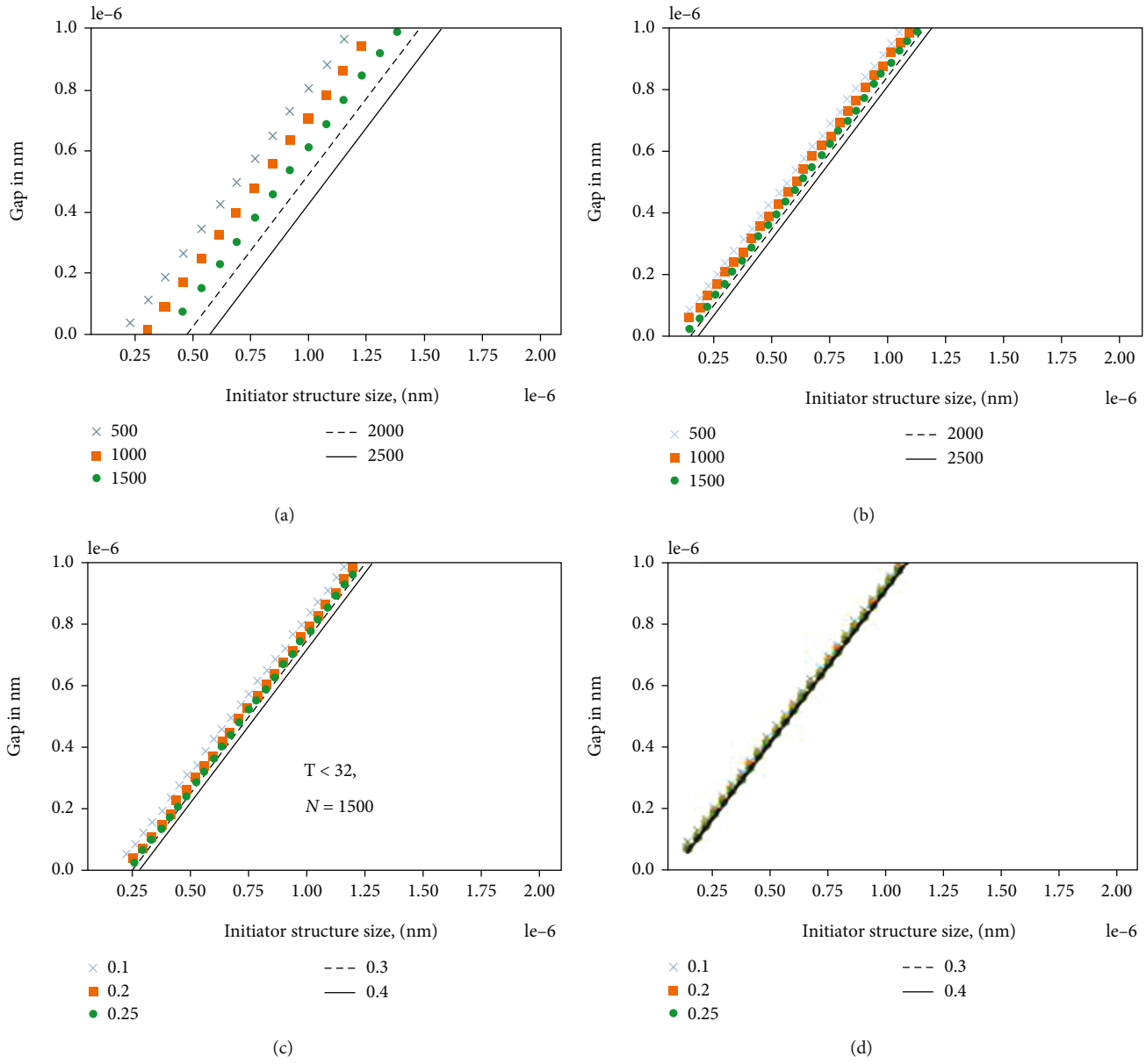


Figure 12: Continued.

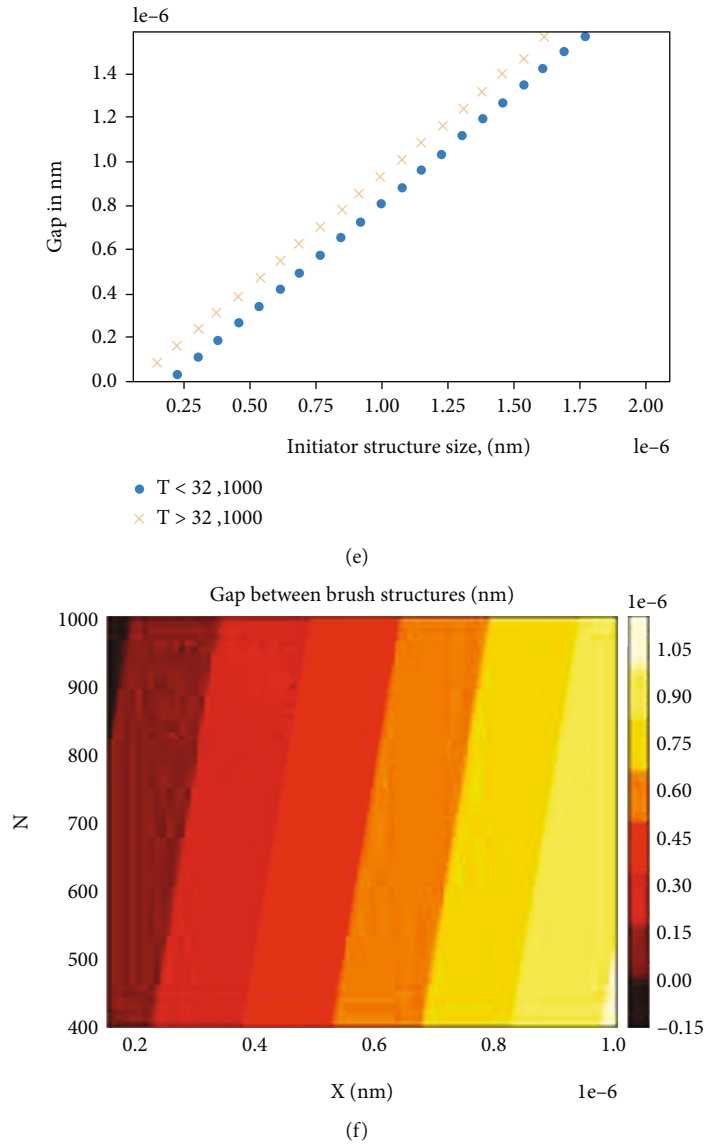


FIGURE 12: Plot of the gap between periodically placed polymer brush structures versus the initiator structure size x; (a) below the LCST for different degrees of polymerization; (b) above the LCST for different degrees of polymerization; (c) below the LCST for different densities; (d) above the LCST for different density; (e) comparison for below the LCST and above the LCST for $N = 1500$; and (f) contor plot of the gap as a function of both $N$ and $x$ while density kept constsnt at 0.4.

the bare substrate. The height is not uniform for the polymer brush structure, instead it decreases from maximum to zero when moving away from the center of the polymer brush structure to the rim of the structure. Figure 7(d) is a plot of the density of the polymer chains as a function of height of the polymer brush structure. The density decreases when moving away from the substrate due to relaxation. Figure 7(e) is a plot of the height of the polymer brush structure as a function of the initiator structure size. The theoretical plot is in good agreement with the experimental plot, Figure 7(a).

To investigate the effect of patterning on the antifouling nature of the surface, the steric repulsive force for patterned (Equation (20)) PNIPAM brushes was plotted as a function of the initiator structure size. The modified equilibrium thickness of the patterned polymer brush (Equation (26)) was substituted in Equation (20), and the nonequilibrium thickness was taken as $L_p$-0.3 nm. Figure 7(f) is a plot of the repulsive force versus initiator structure size for different degrees of polymerization and density. The repulsive force increases as both the degree of polymerization and density increase for a given initiator structure size. When the initiator structure size decreased, the repulsive force decreased and finally becomes almost zero for all degrees of polymerization and density for the initiator structure size less than 200 nm. This is because small pattern sizes produce small thickness regardless of the degree of polymerization and density. From the figure, it is evident that brushes patterned with initiator structure size less than 200 nm may not be effective in preventing the deposition of biomaterials.

Table 2: Values of the gap ($g$) for a given degree of polymerization ($N$), density ($\sigma$), and initiator structures size ($x$).

| | $x$ (nm) | $N$ | | $g$ (nm) | |
|---|---|---|---|---|---|
| | | $\sigma = 0.2$ | $\sigma = 0.4$ | $\sigma = 0.2$ | $\sigma = 0.4$ |
| 1 | 150 | 400 | 325 | 9.6 | 6.3 |
| 2 | 200 | 550 | 450 | 7 | 1.0 |
| 3 | 300 | 850 | 675 | 1.7 | 1.5 |
| 4 | 400 | 1125 | 900 | 5 | 2.1 |
| 5 | 500 | 1400 | 1125 | 8.7 | 2.6 |
| 6 | 600 | 1700 | 1350 | 3.5 | 3.1 |
| 7 | 700 | 1975 | 1575 | 7 | 3.7 |
| 8 | 800 | 2275 | 1800 | 1.7 | 4.2 |
| 9 | 900 | 2550 | 2025 | 5.1 | 4.7 |
| 10 | 1000 | 2845 | 2250 | 1.7 | 5.3 |

*3.4. Chain Bridging between Neighboring Polymer Brush Structures.* To investigate the dependence of the excess width on the initiator structure size, the polymer brush structure size ($d_{pb}$) and initiator structure size ($x$) were digitized from references [15, 16, 19, 21]. The excess width was calculated from the relation

$$w = \frac{1}{2}\left(d_{pb} - x\right). \tag{28}$$

Figures 8(a)–8(d) are plots of excess width versus initiator structure size. As can be seen, the excess width is independent of the initiator structure size and is equal to the thickness of the homogeneous polymer film [44]. The scaling low was fitted for some of the plots where the degree of polymerization and density were available [45] and the equation fits very well, indicating that the excess width of a polymer brush structure can be calculated for any solvent quality using scaling low (Equations (9) and (10)).

Figure 9(a) is a plot of the excess width (Equation (21)) of a polymer brush structure versus the degree of polymerization for different densities. The excess width is strongly dependent on the degree of polymerization and density. The lateral extension converges at a low degree of polymerization for all densities. The effect of the density on the lateral extension is not as significant as the effect of the degree of polymerization. Figure 9(b) is plot of the horizontal component (Equation (21)) of a polymer chain in the structure as a function of the tilting angle. The horizontal component is given in terms of % of equilibrium thickness, and the angle is given in radians. As the tilting angle increases, that is, as the grafting site moves away from the center of the polymer brush structure, the horizontal component increases and finally becomes equal to the equilibrium thickness. This indicates that the polymer chains at the rim of a polymer brush structure lays horizontally to the bare substrate. Therefore, for periodically arranged small polymer brush structures, for example, brushes patterned using interference lithography, neighboring structures may merge due to chain overlap. Figure 10(a) is a python contour plot of a two-beam interference used to produce periodically arranged polymer structures, and Figure 10(b) is a schematic that depicts the change in the gap between the polymer structures due to a change in solution temperature.

Experimental investigation of the effect of solvent on the excess width and consequently on the gap between neighbouring polymer brush structures was examined after patterning PNIPAM brushes on silicon oxide. Figure 11 is an atomic force microscopy image of PNIPAM brush patterned with a period of 270 nm using interference lithography. Figure 11(a) is the atomic force microscopy image of the PNIPAM brush structure above the LCST, and Figure 11(b) is below the LCST. The PNIPAM brush structure period was intentionally made large compared to the thickness of the polymer brush structure (60 nm) to show the width change when the medium temperature is changed from 25°C to 36°C. The width changed from 100 above the LCST to 136 below the LCST. The peak-to-valley distance also changed from 60 nm above the LCST to 20 nm below the LCST. The change in width and the peak to valley distance is due to chain relaxation when the brush is in water at 25°C which shows that the polymer brush structures extend more in to the bare substrate when immersed in a good solvent.

Theoretically, it is possible to determine the gap between periodically patterned polymer brush structures by subtracting twice of the excess width from the initiator structure size. Equation (27) is the expression for the gap between neighboring polymer brush structures ($g = x - 2w$) as a function of the initiator structure size, $x$.

$$g = x - 2l \text{ or } g = x - 2\left(\left(\frac{k_1}{k_2}\right)^{1/4} \mathrm{aN}\sigma^{1/2}\right). \tag{29}$$

Figures 12(a) and 12(b) are plots of the gap between periodically placed polymer brush structures versus the initiator structure size $x$ above and below the LCST for different degrees of polymerization, respectively. As the polymerization increases, the gap decreases since longer chains extend more into the bare substrate. Figures 12(c) and 12(d) are plots of the gap between periodically placed polymer brush structures versus the initiator structure size, x above and below the LCST for different grafting densities, respectively. As the density increases, the gap decreases slightly since more dense polymer brush structures relax to the bare substrate than less dense polymer brush structures. However, when compared to the effect of the degree of polymerization, the effect of density is insignificant since the chains relax to the bare substrate in a good solvent regardless of the density. Figure 12(e) is comparison of the gap between polymer brush structures below the LCST and above the LCST. The gap between the polymer brush structures below the LCST is higher than the gap between the brush structures above the LCST. Figure 12(f) is a contour plot of the gap as a function of both the degree of polymerization and initiator structure size for a density equal to 0.4. This plot was used to prepare Table 2 which lists the value of the gap ($g$) for a given degree of polymerization ($N$), density ($\sigma$), and initiator structures size ($x$).

## 4. Conclusion

This paper showed that the steric repulsive force is affected by patterning, and it depends on the initiator structure size. Small polymer brush structures may not produce sufficient repulsive force to protect the surface from fouling. The functionality of smart nanopores or nanochannels is based on the reversible expansion and collapse of responsive polymers, which provides fouling character when collapsed and antifouling when expanded. Therefore, when fabricating switchable surfaces, it was shown that the minimum initiator structure size has to be determined so that the polymer structure retains its antifouling nature. The second parameter was the excess width, especially for periodically arranged polymer structures. It was shown that chains may overlap if the gap between neighboring polymer brush structures is small compared to the polymer chain length. Therefore, in this work, it was indicated that determination of the gap is essential when fabricating switchable surfaces.

## Data Availability

The data used to support the findings of this study are available from the corresponding author upon request.

## Conflicts of Interest

The author declares that there are no conflicts of interest regarding the publication of this paper.

## Acknowledgments

The author acknowledges the International Science Program (ISP), Sweden and Bahir Dar University, Ethiopia for financial support, and Duke University, USA, for instruments for carrying out interferometric lithography experiments.

## References

[1] S. Ohya, H. Sonoda, Y. Nakayama, and T. Matsuda, "The potential of poly(-N-isopropylacrylamide) (PNIPAM)-grafted hyaluronan and PNIPAM-grafted gelatin in the control of post-surgical tissue adhesions," *Biomaterials*, vol. 26, no. 6, pp. 655–659, 2005.

[2] M. Yoshizawa and H. Ohno, "Polymer brushes," *Electrochemical Aspects of Ionic Liquids*, pp. 363–374, 2005.

[3] M. Müller, "Polymers at interfaces and surfaces and in confined geometries," *Polymer Science: A Comprehensive Reference*, vol. 1, 2012.

[4] S. Ma, X. Zhang, B. Yu, and F. Zhou, "Brushing up functional materials," *NPG Asia Materials*, vol. 11, no. 1, 2019.

[5] T. B. McPherson, S. J. Lee, and K. Park, "Analysis of the prevention of protein adsorption by steric repulsion theory," *ACS Symposium Series*, vol. 602, pp. 395–404, 1995.

[6] D. Leckband, "Measuring the forces that control protein interactions," *Annual Review Of Biophysics And Biomolecular Structure*, vol. 29, no. 1, pp. 1–26, 2000.

[7] S. Lowe, N. M. O'Brien-Simpson, and L. A. Connal, "Antibiofouling polymer interfaces: poly(ethylene glycol) and other promising candidates," *Polymer Chemistry*, vol. 6, no. 2, pp. 198–212, 2015.

[8] A. Malshe, K. Rajurkar, A. S. Hans, N. Hansen, and S. B. WenpingJiang, "Bio-inspired functional surfaces for advanced applications," *CIRP Annals*, vol. 1, no. 62, pp. 607–628, 2013.

[9] S. Patel, M. Tirrell, and G. Hadziioannou, "A simple model for forces between surfaces bearing grafted polymers applied to data on adsorbed block copolymers," *Colloids and Surfaces*, vol. 31, pp. 157–179, 1988.

[10] S. I. Jeon, J. H. Lee, J. D. Andrade, and P. G. De Gennes, "Protein–surface interactions in the presence of polyethylene oxide: I. Simplified theory," *Journal of Colloid and Interface Science*, vol. 142, no. 1, pp. 149–158, 1991.

[11] E. P. K. Currie, W. Norde, and M. A. C. Cohen Stuart, "Tethered polymer chains: surface chemistry and their impact on colloidal and surface properties," *Advances In Colloid And Interface Science*, vol. 100, p. 102, 2003.

[12] H. Suginome and T. Uchida, "Synchronous skeletal rearrangement ofD- nor-5$\alpha$-androstane-16$\alpha$- and -16$\beta$-carbonyl m-chlorobenzoyl peroxides," *Journal of the Chemical Society, Perkin Transactions 1*, vol. 142, no. 1, pp. 943–946, 1980.

[13] J. N. Israelachvili and R. M. Pashley, "Measurement of the hydrophobic interaction between two hydrophobic surfaces in aqueous electrolyte solutions," *Journal of Colloid and Interface Science*, vol. 98, no. 2, pp. 500–514, 1984.

[14] J. Klein and P. F. Luckham, "Forces between two adsorbed poly(ethylene oxide) layers in a good aqueous solvent in the range 0-150 nm," *Macromolecules*, vol. 17, no. 5, pp. 1041–1048, 1984.

[15] W. L. Chen, M. Menzel, O. Prucker, E. Wang, C. K. Ober, and J. Rühe, "Morphology of nanostructured polymer brushes dependent on production and treatment," *Macromolecules*, vol. 50, no. 12, pp. 4715–4724, 2017.

[16] H. Agheli, J. Malmström, P. Hanarp, and D. S. Sutherland, "Nanostructured biointerfaces," *Materials Science and Engineering: C*, vol. 26, no. 5–7, pp. 911–917, 2006.

[17] Y. Wei, Y. Xu, A. Faraone, and M. J. A. Hore, "Local structure and relaxation dynamics in the brush of polymer-grafted silica nanoparticles," *ACS Macro Letters*, vol. 7, no. 6, pp. 699–704, 2018.

[18] A. M. Jonas, Z. Hu, K. Glinel, and W. T. S. Huck, "Effect of nanoconfinement on the collapse transition of responsive polymer brushes," *Nano Letters*, vol. 8, no. 11, pp. 3819–3824, 2008.

[19] X. Liu, Y. Li, and Z. Zheng, "Programming nanostructures of polymer brushes by dip-pen nanodisplacement lithography (DNL)," *Nanoscale*, vol. 2, no. 12, pp. 2614–2618, 2010.

[20] Q. Yu, P. Shivapooja, L. M. Johnson, G. Tizazu, G. J. Leggett, and G. P. López, "Nanopatterned polymer brushes as switchable bioactive interfaces," *Nanoscale*, vol. 5, no. 9, pp. 3632–3637, 2013.

[21] M. Patra and P. Linse, "Simulation of grafted polymers on nanopatterned surfaces," *Nano Letters*, vol. 6, no. 1, pp. 133–137, 2006.

[22] N. Singh, X. Cui, T. Boland, and S. M. Husson, "The role of independently variable grafting density and layer thickness of polymer nanolayers on peptide adsorption and cell adhesion," *Biomaterials*, vol. 28, no. 5, pp. 763–771, 2007.

[23] P. E. Theodorakis, H. P. Hsu, W. Paul, and K. Binder, "Computer simulation of bottle-brush polymers with flexible backbone: good solvent versus theta solvent conditions," *The Journal Of Chemical Physics*, vol. 135, no. 16, 2011.

[24] W. L. Chen, R. Cordero, H. Tran, and C. K. Ober, "50th anniversary perspective: polymer brushes: novel surfaces for future

materials," *Macromolecules*, vol. 50, no. 11, pp. 4089–4113, 2017.

[25] S. Yamamoto, M. Ejaz, Y. Tsujii, and T. Fukuda, "Surface interaction forces of well-defined, high-density polymer brushes studied by atomic force microscopy. 2. Effect of graft density," *Macromolecules*, vol. 33, no. 15, pp. 5608–5612, 2000.

[26] J. I. Martin and Z. G. Wang, "Polymer brushes: scaling, compression forces, interbrush penetration, and solvent size effects," *The Journal of Physical Chemistry*, vol. 99, no. 9, pp. 2833–2844, 1995.

[27] T. M. Birshtein and Y. V. Lyatskaya, "Polymer brush in a mixed solvent," *Colloids and Surfaces A: Physicochemical and Engineering Aspects*, vol. 86, pp. 77–83, 1994.

[28] R. Turcu, A. Nan, I. Craciunescu, A. E. Ivanov, and P. Zubov, "Smart polymers as surface modifiers for bioanalytical devices and biomaterials : theory and practice," *Russian Chemical Reviews*, vol. 85, no. 6, p. 565, 2016.

[29] I. B. Malham and L. Bureau, "Density effects on collapse, compression, and adhesion of thermoresponsive polymer brushes," *Langmuir*, vol. 26, no. 7, pp. 4762–4768, 2010.

[30] Y. Brasse, M. B. Müller, M. Karg, C. Kuttner, T. A. F. König, and A. Fery, "Magnetic and electric resonances in particle-to-film-coupled functional nanostructures," *ACS Applied Materials & Interfaces*, vol. 10, no. 3, pp. 3133–3141, 2018.

[31] W. K. Lee, M. Patra, P. Linse, and S. Zauscher, "Scaling behavior of nanopatterned polymer brushes," *Small*, vol. 3, no. 1, pp. 63–66, 2007.

[32] G. Tizazu, O. El-Zubir, S. R. J. Brueck, D. G. Lidzey, G. J. Leggett, and G. P. Lopez, "Large area nanopatterning of alkylphosphonate self-assembled monolayers on titanium oxide surfaces by interferometric lithography," *Nanoscale*, vol. 3, no. 6, pp. 2511–2516, 2011.

[33] Newport, "Application note 49: theory of Lloyd's mirror interferometer," *Application Note*, pp. 1–6, 2012.

[34] M. Kaholek, W. K. Lee, S. J. Ahn et al., "Stimulus-responsive poly(N-isopropylacrylamide) brushes and nanopatterns prepared by surface-initiated polymerization," *Chemistry of Materials*, vol. 16, no. 19, pp. 3688–3696, 2004.

[35] K. Mandal, M. Balland, and L. Bureau, "Thermoresponsive micropatterned substrates for single cell studies," *PLoS One*, vol. 7, no. 5, pp. 1–7, 2012.

[36] K. N. Plunkett, X. Zhu, J. S. Moore, and D. E. Leckband, "PNIPAM chain collapse depends on the molecular weight and grafting density," *Langmuir*, vol. 22, no. 9, pp. 4259–4266, 2006.

[37] Y. Yu, B. D. Kieviet, F. Liu et al., "Stretching of collapsed polymers causes an enhanced dissipative response of PNIPAM brushes near their LCST," *Soft Matter*, vol. 11, no. 43, pp. 8508–8516, 2015.

[38] A. M. Jonas, H. Zhijun, K. Glinel, and W. T. S. Huck, "Chain entropy and wetting energy control the shape of nanopatterned polymer brushes," *Macromolecules*, vol. 41, no. 19, pp. 6859–6863, 2008.

[39] W. Meyer, "Steric forces measured with the atomic force microscope," *Langmuir*, vol. 6, pp. 2559–2565, 1999.

[40] C. M. Roth, B. L. Neal, and A. M. Lenhoff, "Van der Waals interactions involving proteins," *Biophysical Journal*, vol. 70, no. 2, pp. 977–987, 1996.

[41] S. A. Parke and G. G. Birch, "Solution properties of ethanol in water," *Food Chemistry*, vol. 67, no. 3, pp. 241–246, 1999.

[42] X. Jia, X. Jiang, R. Liu, and J. Yin, "Poly(N-isopropylacrylamide) brush fabricated by surface-initiated photopolymerization and its response to temperature," *Macromolecular Chemistry and Physics*, vol. 210, no. 21, pp. 1876–1882, 2009.

[43] S. R. Sheth and D. Leckband, "Measurements of attractive forces between proteins and end-grafted poly(ethylene glycol) chains," *Proceedings of the National Academy of Sciences of the United States of America*, vol. 94, no. 16, pp. 8399–8404, 1997.

[44] M. Mathieu, A. Friebe, S. Franzka, M. Ulbricht, and N. Hartmann, "Surface-initiated polymerization on laser-patterned templates: morphological scaling of nanoconfined polymer brushes," *Langmuir*, vol. 25, no. 20, pp. 12393–12398, 2009.

[45] E. Bittrich, S. Burkert, M. Müller, K. J. Eichhorn, M. Stamm, and P. Uhlmann, "Temperature-sensitive swelling of poly(N-isopropylacrylamide) brushes with low molecular weight and grafting density," *Langmuir*, vol. 28, no. 7, pp. 3439–3448, 2012.